Proceedings of the XXIII Conference on Applied Crystallography, Krynica Zdrój, Poland, September 20–24, 2015

Influences of Production Method and Minor Chemical Composition Changes on the Microstructure of the Alloy: $Fe_{62-x}Co_{10}Y_8Mo_xB_{20}$ (where $x = 1$ or 2)

M. Nabiałek* and S. Garus

Institute of Physics, Częstochowa University of Technology, al. Armii Krajowej 19, 42-200 Częstochowa, Poland

In this work, the results of studies concerning the structure of polycrystalline and amorphous alloys are presented. The samples were produced in a single-step production process, using two different production methods, and under a protective argon atmosphere. The quenching speed of the molten alloy was different for each of the production methods. Samples were subjected to analysis using X-ray diffractometry, scanning electron microscopy, and computer tomography. It has been shown that the samples manufactured with a higher cooling rate feature an amorphous structure; on the other hand, the samples obtained using the method with the lower cooling speed consist of crystallites of three crystalline phases with sizes of the order of μm. The amorphous samples exhibited a varied fracture surface as well as an increase in the contribution of pores to their volume, in comparison to the samples obtained at the lower cooling speed.

DOI: 10.12693/APhysPolA.130.1010

PACS/topics: 75.50.–y, 75.50.Kj, 75.30.Ds, 75.20.En, 75.47.Np, 75.50.Bb, 75.60.Ej

1. Introduction

At present, in many branches of industry, research is being conducted in order to find modern functional materials with specific useful parameters. The amorphous, nanocrystalline, and microcrystalline alloys definitely feature within this target group. The amorphous materials consist of a single phase, and are characterised by short-range interactions between their atoms [1]. On the other hand, the nanocrystalline materials are described as two-phase materials, consisting of amorphous and crystalline phases [2]. Alloys featuring a mixture of these two phases could have much better functional parameters in comparison to their fully crystalline or fully amorphous counterparts [3, 4]. The third group of alloys comprises materials featuring a completely crystalline structure, in which the crystallites are of micrometric sizes. In the case of these materials, good functional properties also could be achieved [5]. One of the more interesting groups of the amorphous alloys is that of the FeCoB-based alloys; depending on their chemical composition, these alloys can possess exceptional mechanical and magnetic properties [6]. The crystallisation process occurring in these alloys is usually primary, which means that their crystallisation proceeds in two stages. The changes in the structure and magnetic properties, occurring as a result of a different cooling speed being used during the production process, are visible even without crystalline grains being present in the amorphous matrix. A further improvement in the functional parameters of the alloys could be achieved by their controlled crystallisation [7]. Unfortunately, additional stages of thermal treatment increase the final cost of functional materials. Therefore, from an economical point of view, single-stage production processes recently have become important.

In this paper, studies of the microstructure of the two alloys: $Fe_{62-x}Co_{10}Y_8Mo_xB_{20}$ (where $x = 1$ or 2) are presented. The samples were made using two production methods, which feature different cooling rates.

2. Materials and methods

The alloy samples used in the investigations were produced by two different production methods, characterized by different cooling speeds. The samples with polycrystalline structure were manufactured in the form of discs of approximate thickness 5 mm; this was achieved by unidirectional cooling on a copper plate. The samples with amorphous structure and approximate thickness 0.5 mm were obtained by an injection-casting method, involving the injection of the molten alloy into a cooled copper die. Both the polycrystalline and amorphous samples were produced under a protective argon atmosphere, using high-purity components: Fe — 99.98, Co — 99.998, Y — 99.99, Mo — 99.9999 at.%. The element boron was added in the form of an alloy with known composition: $Fe_{45.4}B_{44.6}$. Analysis of the structure of the samples was performed using X-ray diffractometry, scanning electron microscopy, and computer tomography. X-ray diffraction patterns were obtained using a BRUKER ADVANCE D8 diffractometer. The samples were powdered using a low-energy process, then placed on a rotating table, and scanned within the 2Θ range from 30° to 100°, using a Cu K_λ (1.54056 Å) source. A measurement step of 0.02° per 5 s was used. Analysis of the X-ray diffraction patterns was undertaken using EVA software and an ICDD PDF-4+ Release 2013 database. The average size of the crystallites was estimated using the Scherrer equation

*corresponding author; e-mail: nmarcell@wp.pl

$$D = \frac{\lambda K}{B_0 \cos \Theta}, \tag{1}$$

where K — dimensionless shape factor (taken $K = 0.9$), λ — X-ray wavelength, B_0 — full width at half maximum (taking the background into account), Θ — the Bragg angle.

Images of microstructure fractures for the investigated samples were obtained using a SUPRA 35 (by Zeiss) high-resolution scanning electron microscope (SEM). Fractures, obtained by decohesion, were imaged using the detection of secondary electrons (SE) at the acceleration voltage of 25 kV (a maximum magnification of 25000×). Chemical analysis was performed using an EDAX TRIDENT XM4 energy-dispersive X-ray spectrometer (EDS). Three-dimensional image reconstruction was performed utilizing a BRUKER SkyScan 1172 computer microtomograph, with working voltage 100 kV and current 100 μA (tungsten lamp). The sample rotation step was equal to 0.3° (0°−360°) with a measurement time of 1.2 s per step. The achieved resolution was 2.38 μm. Each of the radiograms was composed of the average of six projections.

3. Results and discussion

On the resulting X-ray diffraction patterns, there are no observable narrow peaks that would be typical of a crystalline structure. The X-ray diffraction patterns obtained for amorphous alloys usually consist of a single, wide maximum, called the "amorphous halo". Figure 1 shows X-ray diffraction patterns for the samples of the investigated alloys obtained by injecting the liquid alloy into the cooled, copper die (Fig. 1a,b), and by a rapid cooling on the copper plate (Fig. 1c,d).

The X-ray diffraction patterns recorded for the samples cooled on the copper plate consist of a low intensity background and clearly visible peaks, indicating the presence of the crystalline structure. The results of the calculations according to Eq. (1) for the samples of the investigated alloys are presented in Table I.

TABLE I

Average grain size for the samples obtained on the copper plate, calculated from the Scherrer equation.

Alloy composition	Estimated average size of the grains D [nm]			
	YB_2	Fe_2Y	αFe	B_6Co_{23}
$Fe_{61}Co_{10}Mo_1Y_8B_{20}$	548	1018	372	273
$Fe_{60}Co_{10}Mo_2Y_8B_{20}$	591	–	356	525

In Fig. 2a and c, the fracture surface is presented for samples of the investigated alloys in the form of plates made by rapid quenching of the liquid material in the copper die. In the same figure, Fig. 2b and d, images are presented for samples produced by rapid quenching on the copper plate. However, within the structural fractures of the samples obtained by injection-casting into the copper die, defects are visible in the form of gas bubbles (black rings) which were not observed in the polycrystalline samples. On the basis of analysis of the fractures of the polycrystalline samples, it was found that the fractures are brittle between the crystalline grains. In the case of the fractures obtained for the samples produced in the copper die, more complex structures were observed.

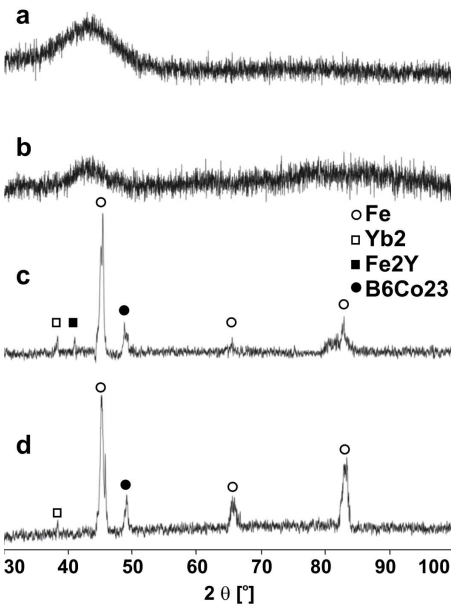

Fig. 1. X-ray diffraction patterns obtained for the samples of the investigated alloys: (a) — $Fe_{61}Co_{10}Mo_1Y_8B_{20}$ and (b) — $Fe_{60}Co_{10}Mo_2Y_8B_{20}$, produced in the copper die and (c) — $Fe_{61}Co_{10}Mo_1Y_8B_{20}$ and (d) — $Fe_{60}Co_{10}Mo_2Y_8B_{20}$, produced on the copper plate.

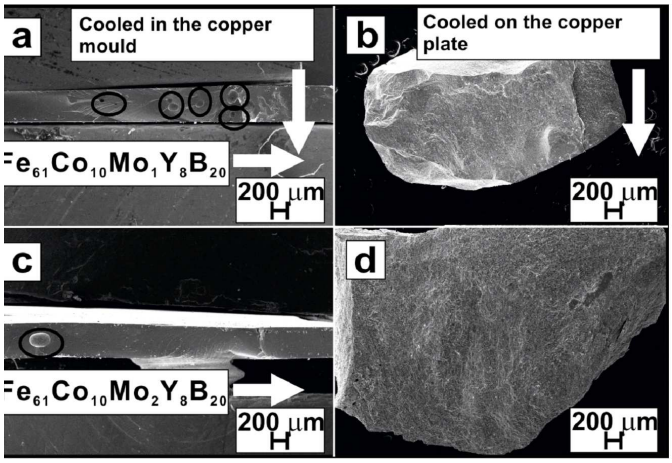

Fig. 2. SEM images for the samples cooled in the copper die (a,c) and on the copper plate (b,d).

In the circle in Fig. 3, it can be seen that on this fracture the scale band starts with a bright divergence, where the origins of the veins are visible. As shown in the marked areas 1–3 of Fig. 3, at the origin of the veins there are areas of varying chemical composition.

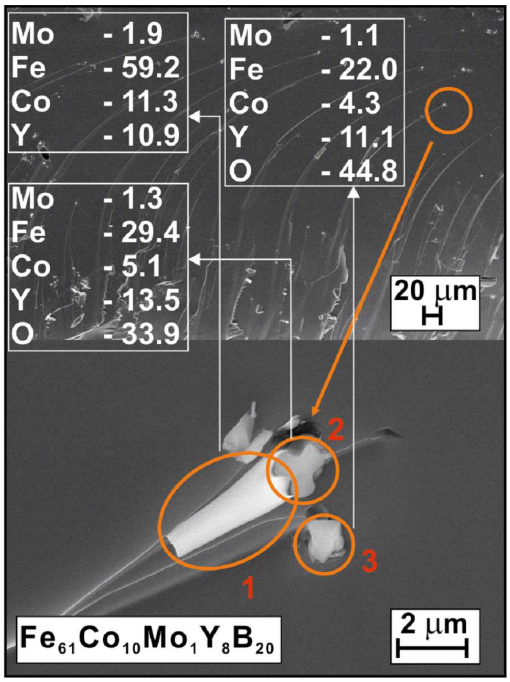

Fig. 3. SEM images of the selected area of the fracture surface of the plate sample and magnification of the indicated section of the $Fe_{61}Co_{10}Mo_1Y_8B_{20}$ alloy, together with X-ray EDS microanalysis of the marked areas 1–3.

The areas in Fig. 3 marked: 1, 2, and 3 represent regions for which X-ray microanalysis of the chemical composition has been performed using EDS. In area 1, as indicated by results of the EDS analysis (Fig. 3, zone 1), the nominal concentration of the alloy elements was found to be present. In areas 2 and 3, the presence of oxides, created during the sample fracturing process, was observed. The presence of structural defects, created during the production process, was investigated using computer tomography. The reconstructed structure images and the percentage of pores for the selected area of the alloy samples, made with two different production methods, are presented in Fig. 4. As can be seen, the structure of the samples made by the injection of liquid alloy into the copper die, is characterised by a more porous structure than that of the samples made by rapid cooling on the copper plate. During the injection process, the molten alloy had been injected into the copper die under a protective argon atmosphere. It is possible that, during the injection process, argon was being mixed with the alloy and becoming trapped during solidification of the alloy. In Table II, details obtained from the computer tomography analysis are presented, giving the percentage contribution of the pores to the alloy volume.

4. Conclusion

The injection-cast samples of both of the investigated alloys were found to possess an amorphous structure. On the other hand, the samples produced at the lower cooling speed were found to have a polycrystalline structure.

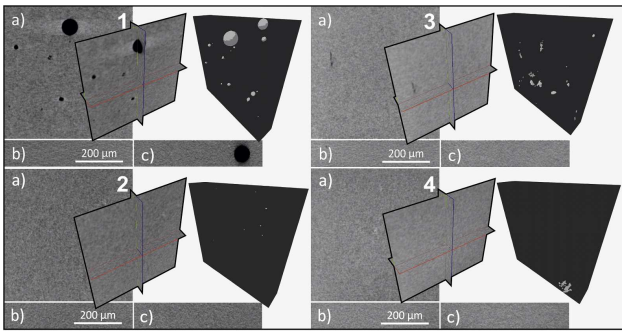

Fig. 4. Reconstructed images of the structures of the $Fe_{62-x}Co_{10}Mo_xY_8B_{20}$ alloys (where $x = 1$ or 2); samples produced by cooling in the copper die (1,3) and on the copper plate (2,4). Cross-sections: sagittal (a), transverse (b), and arrow (c) and their representation in space. Three-dimensional reconstruction of the amorphous (1,3) and crystalline structure (2,4) with visible closed pores.

TABLE II

The pore-content n [%] and average pore-diameter d [μm], estimated using computer tomography, for the samples cooled in the copper mould and on the copper plate.

Alloy composition	mould		plate	
	n	d	n	d
$Fe_{61}Co_{10}Mo_1Y_8B_{20}$	0.64	115.21	0.0	4.77
$Fe_{60}Co_{10}Mo_2Y_8B_{20}$	0.1	15.67	0.03	10.35

During the rapid solidification of the alloy, gas could have been trapped within its volume and pores of larger sizes could have been created, affecting the durability of the resulting material. In the process of fracturing the investigated amorphous materials, microzones with varying chemical composition and high oxygen content were created in the scale-like structure. The deciding factor for the final structure of the studied alloy was found to be the production method: in other words, a minor change in the chemical composition did not have a significant influence.

References

[1] M. Nabiałek, P. Pietrusiewicz, K. Błoch, *J. Alloys Comp.* **628**, 424 (2015).

[2] S. Lesz, R. Szewczyk, D. Szewieczek, A. Bieńkowski, *J. Mater. Process. Technol.* **157-158**, 743 (2004).

[3] A. Inoue, D.V. Louzguine, *Nanostruct. Met. Alloys* **152**, 152 (2011).

[4] M. Nabiałek, *J. Alloys Comp.* **642**, 98 (2015).

[5] A. Inoue, *Acta Mater.* **48**, 279 (2000).

[6] M. Nabiałek, P. Pietrusiewicz, M. Dośpiał, M. Szota, J. Gondro, K. Gruszka, A. Dobrzańska-Danikiewicz, S. Walters, A. Bukowska, *J. Alloys Comp.* **615**, 56 (2014).

[7] D. Szewieczek, S. Lesz, *J. Mater. Process. Technol.* **162-163**, 254 (2005).